Available online at www.sciencedirect.com
ScienceDirect
Geochimica et Cosmochimica Acta 71 (2007) 1021–1040
Geochimica
www.elsevier.com/locate/gca

LA-ICPMS analyses of silicate melt inclusions in co-precipitated minerals: Quantification, data analysis and mineral/melt partitioning

Zoltán Zajacz *, Werner Halter

Department of Earth Sciences, Institute of Isotope Geochemistry and Mineral Resources, ETH Zürich, 8092 Zürich, Switzerland

Received 6 April 2006; accepted in revised form 2 November 2006

Abstract

We present a new approach to determine the composition of silicate melt inclusions (SMI) using LA-ICPMS. In this study, we take advantage of the occurrence of SMI in co-precipitated mineral phases to quantify their composition without depending on additional sources of information. Quantitative SMI analyses are obtained by assuming that the ratio of selected elements in SMI trapped in different phases are identical. In addition Fe/Mg exchange equilibrium between olivine and melt was successfully used to quantify LA-ICPMS analyses of SMI in olivine. Results show that compositions of SMI from the different host minerals are identical within their uncertainty. Thus (1) the quantification approach is valid; (2) analyses are not affected by the composition of the host phase; (3) the derived melt compositions are representative of the original melt, excluding significant syn- or postentrapment modification such as boundary layer effects or diffusive reequilibration with the host mineral. With this data we established a large dataset of mineral/melt partition coefficients for the investigated mineral phases in hydrous calc-alkaline basaltic-andesitic melts. The clinopyroxene/melt and plagioclase/melt partition coefficients are consistent with the lattice strain model of Blundy and Wood [Blundy, J., Wood B., 1994. Prediction of crystal-melt partition-coefficients from elastic-moduli. *Nature* **372**, 452–454].

1. Introduction

Silicate melt inclusions in magmatic minerals provide key information to understand the chemical and mineralogical evolution of igneous systems, provided they preserve the composition of the silicate melt from which the host minerals crystallized. They allow investigation of the origin and the evolution of silicate melts by offering an often unique opportunity to determine the composition of the most primitive melt and monitor the evolution of magmas in the crust through quantification of the relative importance of assimilation, fractional crystallization and contamination processes.

In recent years electron microprobe (EPMA) and Secondary Ion Mass Spectrometry (SIMS) were the most commonly used analytical techniques to measure compositions of SMI for major and trace elements, respectively (Lowenstern, 1995; Schiano, 2003; Pettke et al., 2004). Both SIMS and EPMA require surface exposed and polished SMI which were first homogenized and quenched to a homogenous glass. Thus, they require time consuming sample preparation and allow measurement of only a small part of the SMI present in the sample. Homogenization of SMI can often be rather difficult or impossible, due to potential decrepitation or leakage of the SMI upon heating. In addition, diffusive exchange of certain elements between the host and the SMI might modify the composition of the SMI. This may happen during magmatic evolution or during laboratory reheating experiments which are generally carried out under significantly different physico-chemical conditions from those at which the inclusions were entrapped. In the case of H_2O rich SMI it is particularly difficult to reproduce the original melt composition with laboratory heating experiments due to rapid loss of H_2O

* Corresponding author. Fax: +41 44 6321827.
E-mail address: zajacz@erdw.ethz.ch (Z. Zajacz).

0016-7037/$ - see front matter © 2006 Elsevier Inc. All rights reserved.
doi:10.1016/j.gca.2006.11.001

by H diffusion or leakage of the SMI (Danyushevsky et al., 2002). This will result in compositional changes due to: (1) overheating of the inclusions because of increased liquidus temperature; (2) Fe/Mg exchange between SMI and ferromagnesian host minerals to compensate the decreased Fe^{2+} activity in the SMI due to oxidation by diffusive loss of H_2 (this might also affect other elements too with variable oxidation states); (3) selective loss of fluid compatible elements in case of leakage. Difficulties with homogenization prevented the use of SMI to better understand the genesis and evolution of numerous igneous systems.

Laser ablation ICPMS offers a unique opportunity to analyze the bulk composition of recrystallized SMI without homogenization through heating. It was first successfully applied to glassy, surface exposed SMI (Taylor et al., 1997; Kamenetsky et al., 1998), followed by the application on recrystallized SMI in chemically simple host minerals (quartz and topaz) (Günther et al., 1998; Audetat, 2000; Audetat et al., 2000). Halter et al. (2002) developed an approach that allows measurement of unexposed and recrystallized SMI in chemically complex minerals, greatly increasing the number of inclusions that can be analyzed in the same crystal. The technique is based on ablating entire SMI along with its host mineral and subsequent deconvolution of the mixed ablation signal. Since exposure of the SMI is not necessary, this technique allows analysis of numerous SMI from the same inclusion assemblages allowing critical evaluation of the data and recognition of accidental entrapment of other phases (fluid or mineral) along with the melt, or potential boundary layer effects. Moreover as SMI do not need to be homogenized, potential problems associated with the homogenization step are avoided. This enables the use of melt inclusions in many magmatic systems which were not accessible to SMI investigations with commonly used techniques.

The downside of the approach developed by Halter et al. (2002) is that it requires an internal standard (an element with known concentration in the SMI) to determine the relative contribution of the host mineral and the melt inclusion to the mixed laser ablation signal. An internal standard is difficult to obtain but essential for the quantification of the measurement.

In this study, we show that combining analyses of SMI in different co-precipitated host minerals allows quantification of the LA-ICPMS analyses without having to rely on additional information for the internal standard. We analyzed silicate melt inclusions in co-precipitated olivine, clinopyroxene and plagioclase phenocrysts in an erupted basaltic andesite from the Villarrica volcano (Southern Chile). The major goals of the study are threefold: (1) to develop a stand alone, widely applicable approach to quantify SMI compositions with LA-ICPMS; (2) to evaluate if there is significant postentrapment modification in the concentration of specific elements in the inclusions form various host minerals; (3) to establish an internally consistent dataset of mineral/melt partition coefficients for numerous major and trace elements in the hydrous basaltic andesite from Villarrica. The petrogenetic interpretation of the SMI data is beyond the scope of this paper.

2. Sample selection and petrography

The major criteria used to select the appropriate volcanic rock for this study was to find clear textural evidence for the co-precipitation (cotectic crystallization) of at least two magmatic minerals containing SMI. We eventually selected a sample where co-precipitation of three mineral phases occurred during a significant interval of crystallization which enables a test of the range of applicability of the technique, and a comparison of the results from SMI from several host minerals. The sample is a fresh basaltic-andesite from a late Holocene lava flow deposited on the top of the Pucón Ignimbrite sequence of the Villarrica volcano. This rock has a finely crystallized matrix and contains approximately 10–20 vol% of phenocrysts (plagioclase > olivine > clinopyroxene). Intergrowths of plagioclase–clinopyroxene, plagioclase–olivine, olivine–clinopyroxene and olivine–plagioclase–clinopyroxene was observed by optical microscopy and back scattered electron imaging, providing clear evidence for their co-precipitation (Fig. 1).

Plagioclase contains abundant, mostly isometric or slightly elongated SMI with a wide size distribution between 5 and 65 μm. All SMI in plagioclase are recrystallized to a fine grained mineral assemblage (Fig. 2a).

Olivine generally contains individual melt inclusions in much lower abundance than the plagioclase. The size of the SMI in olivine is highly variable ranging from 10 to 120 μm, most of them being between 15 and 50 μm (Fig. 2). They are isometric or slightly elongated elliptical in shape. The degree of recrystallization varies from almost glassy inclusions (Fig. 2b) to partly recrystallized inclusions with microscopically distinguishable daughter phases (Fig. 2c). In addition to SMI, olivine contains abundant Cr–Mg rich spinel inclusions. Cr–spinel of similar composition is also present as independent phenocrysts in the matrix.

SMI in clinpyroxene are rare, they are usually isometric or slightly elongated and contain small daughter crystals in a transparent residual glass (Fig. 2d). Their size ranges from 15 to 55 μm.

3. Analytical techniques

Table 1 provides a summary of the analytical conditions and data acquisition parameters used for LA-ICPMS analysis. The system consists of a 193 nm ArF excimer laser with an energy homogenized beam profile (Günther et al., 1997) coupled with an ELAN 6100 ICP quadrupole mass spectrometer. The laterally homogenous energy density of the laser beam allows controlled ablation with a flat bottomed ablation crater. The ablation rate was between 0.12 and 0.16 μm/pulse for all analyzed minerals and glasses. The system permits online observation of the ablation

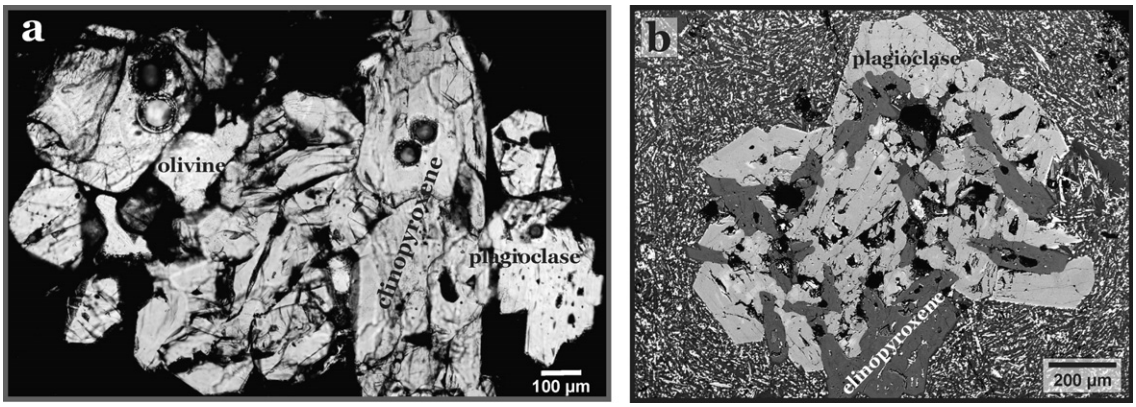

Fig. 1. (a) Microphotograph of olivine + clinopyroxene + plagioclase showing tight intergrowth (transmitted light); (b) back scattered electron image of a plagioclase–clinopyroxene intergrowth.

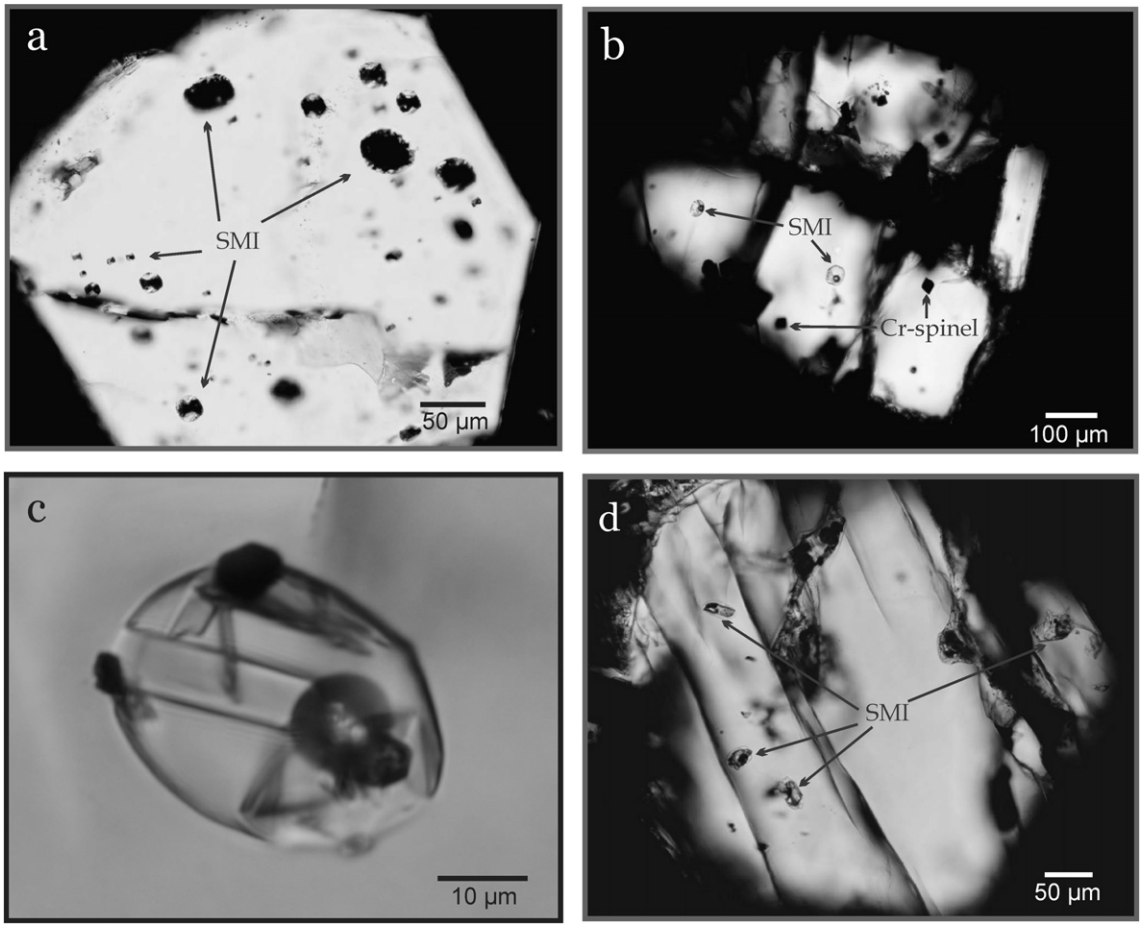

Fig. 2. (a) Recrystallized SMI in a plagioclase phenocrysts; (b) Glassy SMI and Cr–spinel inclusions in olivine; (c) recrystallized SMI in olivine; (d) recrystallized SMI in clinopyroxene.

signal which is a prerequisite for controlled SMI analysis. Analyses of 16 unknowns were bracketed by measurement of an external standard (NBS SRM 610) to allow linear drift correction. Linear dynamic range of 8 orders of magnitude of the detector in the ELAN 6100 allows simultaneous measurement of major and trace elements (down to sub-ppm level). This allows quantification of the measurements by normalizing the concentration of the major elements to 100 wt% using the relative sensitivity factors (signal intensity/concentration in the sample) determined for each elements with the external standard. The BCR-2g glass standard, which has a similar major element composition as the melt inclusions, was repeatedly analyzed as unknown during the measurement sessions to test the accuracy of the system. An average analysis of the BCR-2g standard (obtained by normalizing major elements to a

Table 1
LA-ICPMS analytical conditions

Excimer 193-nm ArF laser Complex 110I	
Output energy	80–85 mJ
Energy density on sample	~10 J/cm^2, homogenous energy density
Pulse duration	15 ns
Repetition rate	10
Pit sizes	Between 14 and 90 μm
Ablation cell volume	8 cm^3
Cell gas flow	1.0 l/min He
Elan 6100 quadrupole ICP-MS	
Nebulizer gas flow	0.72–0.83 l/min
Auxiliary gas flow	0.75 l/min
Cool gas flow	14–15 l/min
RF power	1350 V
Detector mode	Dual, 8 order of magnitude linear dynamic range
Quadropole settling time	3 ms
Data acquisition parameters	
Sweeps per reading	1
Readings per replicate	200–350
Replicates	1
Dwell time per isotope	20 ms for Nb, Ta, Yb and Lu, 10 ms for all others
Points per peak	1 per measurement
Oxide production rate	Tuned to <0.5% ThO
Isotopes analyzed	^{7}Li, ^{11}B, ^{23}Na, ^{25}Mg, ^{27}Al, ^{29}Si, ^{31}P, ^{39}K, ^{42}Ca, ^{45}Sc, ^{49}Ti, ^{51}V, ^{53}Cr, ^{55}Mn, ^{57}Fe, ^{62}Ni, ^{65}Cu, ^{85}Rb, ^{88}Sr, ^{89}Y, ^{90}Zr, ^{93}Nb, ^{133}Cs, ^{137}Ba, ^{139}La, ^{140}Ce, ^{141}Pr, ^{146}Nd, ^{147}Sm, ^{151}Eu, ^{157}Gd, ^{159}Tb, ^{165}Ho, ^{173}Yb, ^{175}Lu, ^{178}Hf, ^{181}Ta, ^{208}Pb, ^{232}Th ^{238}U

100%) is shown, and compared to the certified data in Table 2.

Time-dependent elemental fractionation during ablation has been shown to be minimal with the use of a 193 nm ArF excimer laser and a He gas flow in the ablation chamber. They generate, respectively, a narrow particle size distribution and reduced particle deposition in the ablation chamber (Günther et al., 1997; Günther and Heinrich, 1999a,b; Günther et al., 2001; Guillong and Gunther, 2002; Guillong et al., 2003a,b). This is a crucial issue for SMI analysis as small errors on the compositions induce an enlarged effect on the resulted element concentrations in SMI due to the quantification through extrapolation from the mixed host + inclusion signal. Thus even a small degree of fractionation might significantly affect the determination of compatible elements which are present in a much higher concentration in the host mineral than in the SMI. To reduce any potential elemental fractionation effect in the ablation crater, melt inclusions were ablated using manual active focusing (i.e., the laser beam is always focused on the bottom surface of the ablation crater by moving the sample stage of the microscope). This is important in the case of small (<20 μm) and relatively deep seated inclusions (deeper than half their diameter) where the crater depth/diameter ratio becomes large at the end of the analysis.

Magmatic phenocrysts have also been analyzed for their major element composition by a JEOL SUPERPROBE JXA-8200 electron microprobe at ETH-Zürich. A 15 kV acceleration voltage and a 15 nA beam current were used. Counting times of 20 s on the peak and 10 s on the background on both sides were used for each element.

To obtain a bulk rock composition, XRF analyses were carried out for major elements. In addition to the XRF analyses, a small amount (about 1 g) of rock powder was molten and held at 1300 °C for 1 h in a Pt crucible at ambient pressure, and subsequently quenched. The resulting glass was analyzed by EPMA for major elements and by LA-ICPMS for major and trace elements. Consistency of multiple analyses with the latter two methods granted the homogeneity of the glass. Na_2O and K_2O concentrations from XRF and EPMA are consistent, indicating that volatile elements were not lost during melting of the powder. This is further supported by the fact that the weight of the starting powder and the quenched glass were identical within a 0.1‰ relative error.

4. Bulk rock and mineral compositions

The studied rock sample is a calc-alkaline basaltic andesite (Table 2). Its trace element composition is typical for island arc settings, exhibiting strong negative Nb and Ta and positive LILE anomalies (Fig. 3).

Despite the relatively high SiO_2 content of the rock (SiO_2 = 57 wt%), phenocrysts display a primitive composition. Plagioclase is highly calcic, the anorthite content ranges from 87% to 77%. The magnesium number (mg#) of the olivine varies between 87 and 78. The chromium number (cr#) of spinel inclusions in olivine and spinel phenocrysts is between 37 and 46. The clinopyroxene is CaO rich (18.9–22.4 wt%)

Table 2
Whole rock composition and average analysis of BCR-2g glass standard compared to the certified composition

	BCR-2g			Bulk rock			
				Glass			XRF pellet
	Certified	Measured (7)	Uncertainty (%)	LA-ICPMS (9)	Uncertainty (%)	EPMA (16)	XRF (1)
SiO_2	55.0	55.7	0.47	57.3	1.97	56.6	57.3
TiO_2	2.32	2.04	2.38	0.99	3.80	1.09	1.14
Al_2O_3	13.1	13.4	0.40	15.9	3.09	15.8	16.0
FeO	12.4	12.0	1.17	7.46	2.47	7.42	7.18
MnO	0.21	0.19	1.19	0.14	2.52	0.14	0.15
MgO	3.57	3.39	1.28	4.23	3.01	4.41	4.32
CaO	7.1	6.95	2.01	7.02	3.98	7.00	7.25
Na_2O	3.14	3.19	1.01	4.09	2.03	3.47	3.50
K_2O	1.77	1.83	2.76	1.04	3.55	1.07	1.03
P_2O_5	0.37	0.29		0.29	1.79	0.35	0.35
Total	98.61	98.61		98.24		97.42	98.24
P	1615.5	1281	1.71	1295	1.79		
Sc	31.8	31.2	2.92	23.1	4.10		
V	414.0	421	1.69	158	2.83		
Cr	18.8	16.0	4.25	96.9	8.85		
Ni	13.0	15.4	8.86	85.0	8.95		
Cu	15.5	18.1	4.72	55.3	8.72		
Rb	47.0	50.1	1.97	27.2	1.78		
Sr	342	322	3.57	393	3.60		
Y	36.9	31.3	4.44	26.9	14.18		
Zr	188	169	4.07	117	6.38		
Nb	12.3	10.6	3.61	2.4	3.59		
Ba	683	637	2.76	270	4.20		
Cs	1.1	1.2	2.69	3.5	4.38		
La	25.0	25.3	3.47	11.0	4.19		
Ce	53.3	51.4	3.76	25.7	4.71		
Pr	6.6	6.3	2.98	3.4	6.49		
Nd	28.9	27.7	2.89	16.6	4.88		
Sm	6.6	6.3	3.30	4.2	3.89		
Eu	2.0	2.0	6.05	1.2	6.78		
Gd	6.7	5.8	9.22	4.1	8.10		
Tb	1.1	1.0	7.24	0.7	5.51		
Ho	1.3	1.2	9.75	0.9	5.65		
Yb	3.4	3.3	5.56	2.6	4.21		
Lu	0.50	0.47	4.05	0.37	6.99		
Hf	5.1	4.5	5.40	3.1	4.25		
Ta	0.76	0.57	5.85	0.24	10.42		
Pb	10.6	11.0	3.99	9.4	4.79		
Th	6.1	5.6	4.33	2.2	5.25		
U	1.7	1.7	3.23	0.8	7.71		
Li	9.6	10.4	1.83	15.2	3.77		

Major elements in wt%, trace elements in ppm. Certified values of BCR-2g composition are from Rocholl (1998) for major and from Jochum et al. (2005) for trace elements. LA-ICPMS analyses are normalized to the total of certified (BCR-2g) or XRF (bulk rock) data.

and its mg# (using FeO_t) decreases from 85 to 79 with the decrease of the Cr_2O_3 content from 0.8 to 0.2 wt%.

In most phenocrysts, narrow rims of a more evolved composition were observed. In plagioclase, this overgrowth displays significantly lower anorthite contents (from 60% to 70%), in olivine, more iron rich compositions with mg# of 72–74 were identified. Spinel generally has a narrow Cr-poor, iron rich overgrowth. These overgrowths did not contain silicate melt inclusions.

5. Quantification of SMI analyses

Analyses of SMI and quantification of their composition were based on the method described by Halter et al. (2002). The principles of the quantification and uncertainty estimation are discussed there and we provide only a brief description herein. The technique is based on the ablation of entire SMI with their host mineral, using the smallest beam size possible to ablate the entire melt inclusion. The collected signal consists of a contribution form the SMI and the host mineral. To obtain the composition of the SMI, we need to subtract the contribution of the host mineral from the mixed signal (Fig. 4). This requires that (1) the composition of the host is known and (2) the relative contribution of the host and the SMI to the bulk signal can be quantified.

The composition of the host mineral can be derived from the ablation signal before or after the melt inclusion,

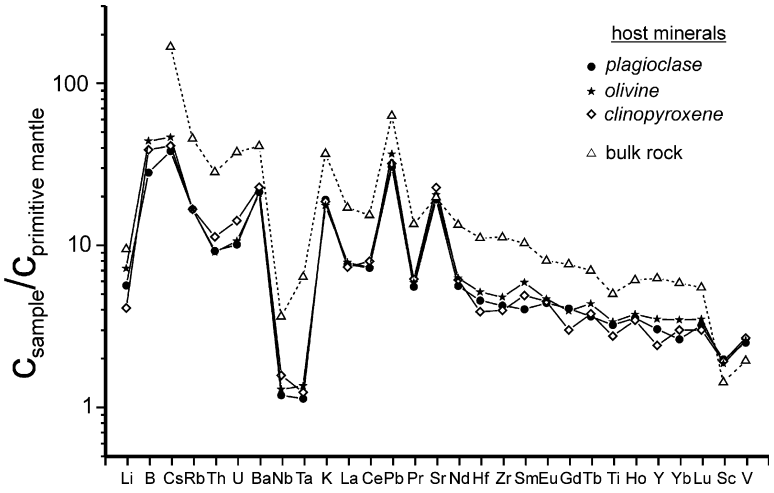

Fig. 3. Primitive mantle normalized spider diagram of SMI and bulk rock. SMI show consistent trace element patterns regardless of the host minerals. These patterns are similar to those in bulk rocks, although shifted to lower concentrations. The shift is due to the fact that SMI concentrations are taken at the primitive end (Rb = 10 ppm) of the melt evolution.

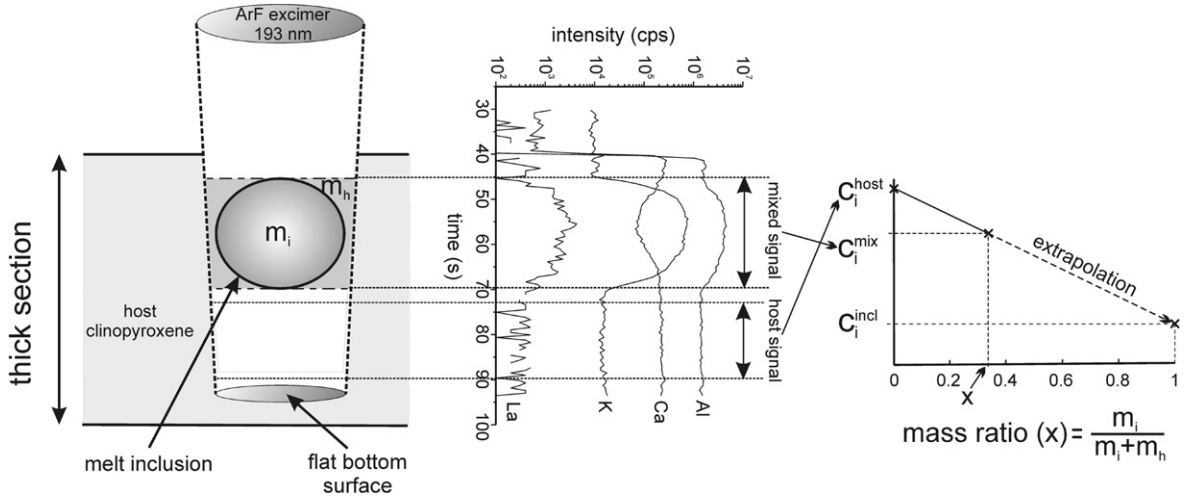

Fig. 4. Schematic representation of SMI analysis by LA-ICPMS. The whole SMI is ablated together with its host mineral, both contributing to the ablation signal in this interval (mixed signal). The composition of the SMI can be calculated through extrapolation from the mixed (melt inclusion + host) composition if the mass ratio of the SMI and host (x) in the ablated volume is known. The composition of the host mineral can be directly calculated from the ablation signal before or after the inclusion (host signal), or from a separated shot next to the inclusion. m_i = mass of the SMI, m_h = mass of the host mineral contributing to the mixed signal, c_i = concentration of a selected element.

or preferably, by analyzing the host mineral right next to the melt inclusion and integrating the ablation signal from the same depth interval as the SMI. This further minimizes the effect of depth induced elemental fractionation during the analysis.

Quantification of the relative contribution of the host and the SMI to the mixed ablation signal has been done previously using an internal standard. An internal standard is an independently determined element or element ratio in the SMI. Different approaches were suggested by Halter et al. (2002) to determine this internal standard. They all suppose information from an external source, which can be (1) EPMA analyses of homogenized SMI from the same assemblage; (2) extensive bulk rock data from the same system providing characteristic element concentrations or ratios; (3) well established mineral/melt partition coefficients in systems with similar composition to the one investigated.

Here, we introduce new alternatives to deconvolute the mixed signal based either on mineral/melt exchange coefficients (SMI in olivine) or on occurrence of SMI in different co-precipitated host minerals (SMI in clinopyroxene and plagioclase). Below, the quantification procedures are discussed separately for SMI trapped in different host minerals.

5.1. Quantification of SMI analyses in plagioclase

Quantification of the plagioclase hosted SMI was based on the textural evidence that olivine and plagioclase

crystallized simultaneously. Based on this observation we can assume that SMI in these two minerals represent the same melt composition or overlapping compositional trends. This assumption will be verified later.

Using elements that are incompatible in olivine we can determine element ratios representing the entrapped melt directly from the mixed analysis of SMI + olivine since the contribution from the host mineral is negligible. Thus, the variation of certain element ratios along the liquid line of descent is given by the analysis of olivine hosted SMI before deconvolution of the host and inclusion signal. As olivine and plagioclase were co-precipitated we can assume that these elements have the same ratios in SMI in plagioclase. Consequently we can iteratively subtract the host plagioclse composition from the mixed analyses of plagioclase hosted SMI to reach the required element ratio characteristic for the melt. With this approach the contribution of the host plagioclase to the bulk signal and the composition of SMI in plagioclase can be calculated. For accurate quantification we use a ratio between a compatible and an incompatible element in plagioclase. This ensures that this ratio is strongly different in the host mineral and the entrapped melt, thus step by step subtraction of the host mineral from the bulk signal results in a rapid change in the apparent element ratio and an accurate determination of the mass ratio (i.e., ratio of the relative contribution of the host mineral and the SMI to the bulk LA-ICPMS signal). In this study we used the Al_2O_3/V ratios obtained from the mixed analyses of the olivine + SMI mixtures to determine the mass ratio for plagioclase + SMI analyses since the Al_2O_3/V ratio is a steep function of the mass ratio (Fig. 5a).

Commonly, silicate melt inclusions from a single mineral phase represent a range of melt compositions along an evolutionary trend. Consequently we cannot assume a fixed element ratio but have to consider changes in the melt composition along the liquid line of descent. We used the ratio of two further elements, sensitive to the degree of crystallization, to monitor melt evolution. The CaO/Na_2O ratio is an ideal candidate due to co-precipitation of calcic clinopyroxene and anorthite rich plagioclase, both characterized by much higher CaO/Na_2O ratio than the silicate melt from which they crystallized. Intersection of the trend in Al_2O_3/V versus CaO/Na_2O defined by olivine hosted inclusions with the trend resulting from step by step subtraction of the host plagioclase composition from the mixed analysis of plagioclase + SMI defines the appropriate mass ratio between the inclusion and the host and allows proper deconvolution and quantification of the SMI compositions in plagioclase (Fig. 5a). It is important to note that the element ratio used for quantification (in this case Al_2O_3/V) must be selected in such a way that its variation is not only due to the crystallization of plagioclase. If this was the case, subtraction of the host mineral from the bulk laser ablation signal would result in a trend similar to the liquid line of descent, as plagioclase is effectively fractionated in both calculations. In the present case V is incorporated in spinel,

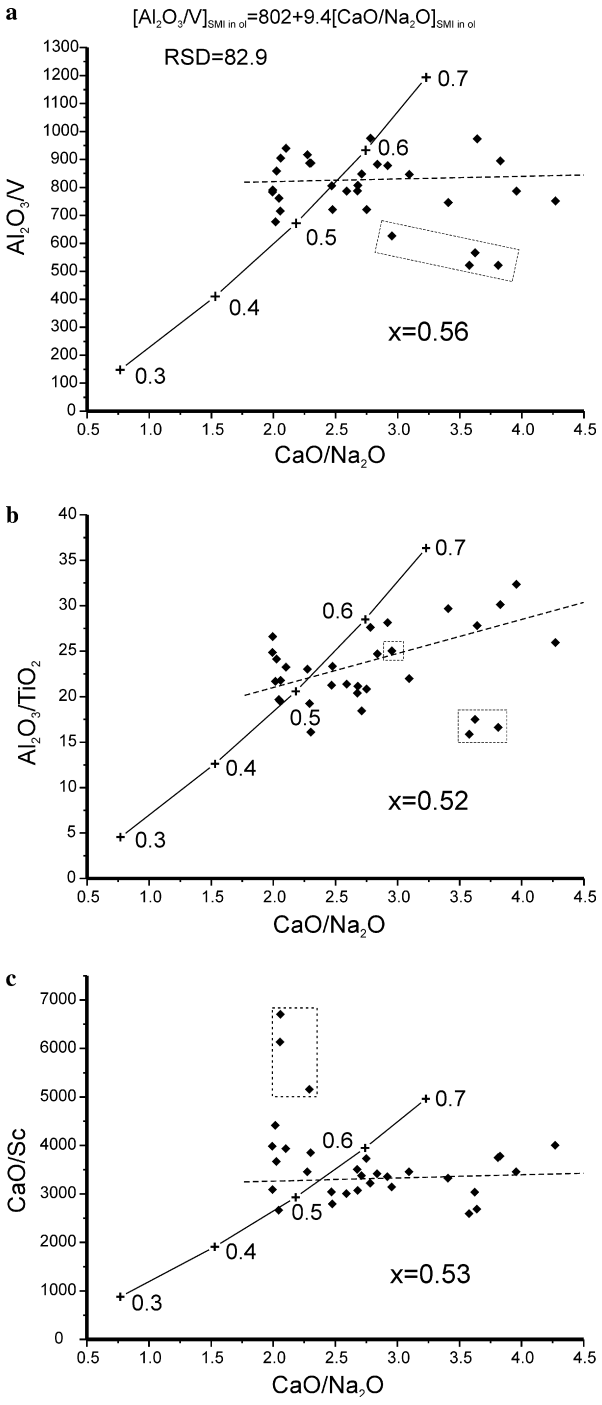

Fig. 5. Examples of determination of the mass ratio for a single plagioclase hosted SMI. The data points sampling the liquid line of descent are derived from olivine hosted SMI. The dashed line is a linear fit to these data, the solid line shows the modeled composition of the single SMI in plagioclase with variable degree of host subtraction from the mixed signal. The values on the line represent the mass ratio (x). Intersection of the lines defines the correct degree of host subtraction. Symbols in rectangles are outlier SMI data derived from a single phenocryst, these have been disregarded for the fitting.

and variation of Al_2O_3/V along the liquid line of descent (deduced from analysis of SMI in olivine) occurs at a high angle with the modeled variation due to plagioclase

removal from the mixed signal of plagioclase hosted SMI (Fig. 5a).

The uncertainty in the deconvolution is given by the standard deviation of the data around the trend defined by the liquid line of descent. Scattering of the results comes from (1) analytical uncertainty and (2) natural variability in the melt composition. Analytical uncertainties in the mixed olivine + SMI signal are generally low, especially for elements present at relatively high concentrations. For Al_2O_3, V, Na_2O and CaO, one standard deviation in the mixed signal is generally below 2% relative. Natural scattering of the data displayed on Fig. 4a is 10% relative at one standard deviation. This has been considered for the uncertainty determination of the single SMI analyses as an uncertainty in the mass ratio. We tested if the use of element ratios other than Al_2O_3/V would result in the same mass ratio. Al_2O_3/TiO_2 and CaO/Sc ratios were selected based on the above detailed criteria. Resulting mass ratios differ by less than 7 relative % (Figs. 5b and c) which is within the uncertainty calculated above.

The SMI compositions are normalized to 100% minus the H_2O content of the melt (H_2O is not detected by LA-ICPMS). We estimated the water content of the melt based on CaO/Na_2O exchange coefficients between plagioclase and melt using data from (Sisson and Grove, 1993b; Sisson and Grove, 1993a), established for silicate melts quite similar in composition to the Villarrica basalts and basaltic-andesites. CaO/Na_2O ratios characteristic for the melt could be obtained from the mixed signal of olivine hosted SMI prior to quantification as both elements are incompatible in olivine. Results scatter around 4 wt% H_2O, thus SMI compositions have been normalized to a total of 96%. This water content was also used to quantify the composition of SMI in other host minerals.

5.2. Quantification of SMI analyses in olivine

To test the validity of the approach based on the coexistence of the mineral phases and the accuracy of the data produced, we used an independent method for the quantification of SMI compositions in olivine. This method does not require the existence of any other co-precipitating phase and can be used in studies dealing with olivine hosted SMI only.

Here, the mass ratio was determined by using the Fe^{2+}/Mg exchange equilibrium between olivine and silicate melt ($Kd^{ol/melt}_{Fe-Mg}$). With this Kd the Fe^{2+}/Mg ratio in the melt can be predicted form the Fe^{2+}/Mg ratio in the host olivine. As the Fe^{2+}/Mg ratio is very different in the melt and the olivine, it is a steep function of the mass ratio. Thus, the host olivine composition can be subtracted iteratively from the mixed olivine + SMI analysis until the predicted Fe^{2+}/Mg ratio is obtained.

A value of 0.31 was used for the $Kd^{ol/melt}_{Fe-Mg}$ based on data of Ulmer (1989) at low pressures (0.1–0.3 GPa). We estimated the $Fe^{2+}/(Fe^{2+} + Fe^{3+})$ ratio in the melt using the method of Kress and Carmichael (1991). Oxygen fugacity values have been estimated by the method of Ballhaus et al. (1991) based on equilibrium Cr–spinel and olivine compositions. Application to 10 spinel–olivine pairs yielded $\log fO_2$ values of FMQ + 1.57 ± 0.26, which corresponds to an $Fe^{2+}/(Fe^{2+} + Fe^{3+})$ ratio of 0.76 ± 0.02.

The FeO/MgO ratio in olivine hosted melt inclusions is known to be influenced by postentrapment modification by continuous reequilibration of the trapped crystallizing melt and the host olivine. The process is described in details by Danyushevsky et al. (2000) and results in an FeO loss and a MgO gain in melt inclusions. The extent of postentrapment Fe-loss depends on the width of the temperature interval over which slow cooling occurred, the amount of olivine that can be crystallized on the inclusion walls in this temperature range and on the degree of equilibration (Danyushevsky et al., 2000). We modeled the potential Fe-loss in melt inclusions using the "Fe-loss" software written by L. Danyushevsky (Danyushevsky et al., 2000). For the model we used 50 °C as an interval of slow cooling with reequilibration and the composition of one of the most primitive SMI trapped in plagioclase. The 50 °C cooling interval resulted in decrease of the mg# of the host olivine from 85 to 82. This range in mg# is wider than the measured difference between core and rim in any of the studied olivine grains. Thus postentrapment modifications are probably less than calculated with the model for the highest degree of reequilibration. Results of the modeling assuming 0%, 50% and 100% reequilibration are shown in Fig. 6. It can be seen that direct quantification of LA-ICPMS would yield compositions with lower MgO and FeO concentrations in the SMI because the Fe-loss causes subtraction of higher amount of olivine from the mixed signal to reach the FeO/MgO ratio dictated by the $Kd^{ol/melt}_{Fe-Mg}$. However the error on the mass ratio is small: approximately 3% relative even for a 100% reequilibration for the most primitive SMI. Certainly this uncertainty would be significantly enlarged in systems where the slow cooling temperature interval is wider and if the melt has a high potential to crystallize ferromagnesian phases. Uncertainty on the $Kd^{ol/melt}_{Fe-Mg}$ also introduces uncertainty on the determination of the mass ratio. This has also been estimated by using an absolute uncertainty of ±0.03 on $Kd^{ol/melt}_{Fe-Mg}$ (most experimental and natural data scatters within this range). This resulted in only a 2.8% uncertainty on the calculated mass ratio. The uncertainty on the mass ratio induced by the uncertainty on Fe^{2+}/Fe^{3+} ratio estimation in the melt is below 0.5% relative. Given these estimations, we used a 3% relative uncertainty on the mass ratio as additional input for calculation of the uncertainties on the single SMI compositions.

5.3. Quantification of SMI analyses in clinopyroxene

Compositional data from SMI in plagioclase and olivine were used to quantify the clinopyroxene hosted SMI. To do this we use the concentration of Al_2O_3 which does not change significantly with melt evolution, but is very

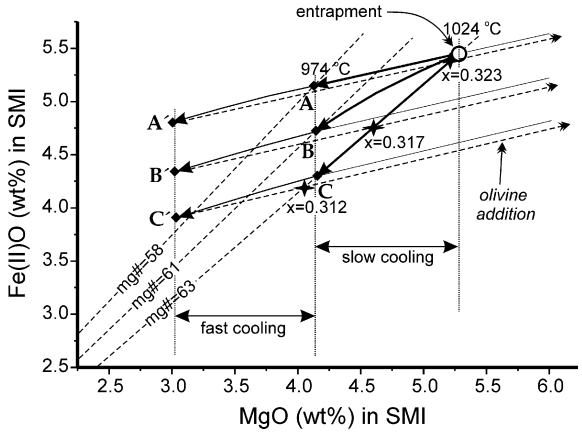

Fig. 6. Model of the uncertainty on the mass ratio for SMI analyses in olivine as a result of potential postentrapment Fe-loss from the inclusions. The opened circle shows the initial composition of the trapped melt used as a starting point for the model. The dashed lines indicate the mg# of the melt in the inclusion. The interval of slow cooling allows different degree of reequilibration (0%—A, 50%—B, 100%—C) between the host olivine and the entrapped melt leading to various degrees of Fe-loss from the inclusion. In the fast cooling interval (to A′, B′ and C′) olivine is still crystallizing on the inclusion walls but there is not enough time for diffusive reequilibration. Dashed arrows show the SMI composition obtained by adding the host olivine to the modified SMI composition (A′, B′ and C′). The intersections (marked by stars) of these arrows with the line representing the melt composition in equilibrium with the host olivine (mg# = 63) defines the mass ratio. Results show that melt compositions derived by quantification of the LA-ICPMS analysis are low in both MgO and FeO because the Fe-loss causes subtraction of higher amount of host mineral (inappropriately low mass ratio) to reach the appropriate Fe^{2+}/Mg ratio However the relative error on the mass ratio is low (in the order of a few relative %). The temperatures shown are estimated by "Fe-loss" algorithm written by L. Danyhusevsky.

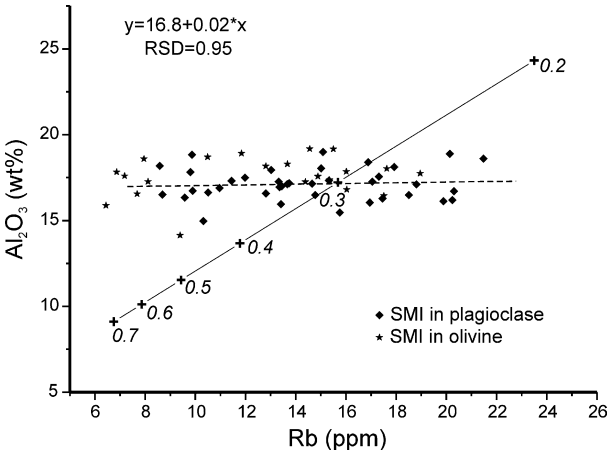

Fig. 7. Quantification of clinopyroxene hosted SMI. Symbols show the melt composition determined in olivine and plagioclase hosted SMI and the dashed line is the regression through these points. The solid line shows the modeled Rb and Al_2O_3 concentrations in SMI from clinopyroxene as a function of various mass ratios between 0.2 and 0.7. The intersection defines the correct mass ratio.

sensitive to the mass ratio in clinopyroxene. We selected Rb as a monitor of melt evolution because it is highly incompatible in all the crystallizing minerals. This implies that concentrations of Rb must increase in the melt with progressing crystallization and that it is not subject to postentrapment modifications in the clinopyroxene. Fig. 7 shows that Al_2O_3 concentrations in plagioclase and olivine hosted SMI do not show significant variations as a function of Rb content. However, the modeled Al_2O_3 content in clinopyroxene hosted SMI is quickly changing with the mass ratio due to its incompatible behaviour. We used the mean Al_2O_3 concentrations obtained from plagioclase and olivine hosted SMI (16.9 wt%) to quantify the composition of clinopyroxene hosted inclusions. Relative standard deviation (RSD) of the Al_2O_3 content of 59 plagioclase and olivine hosted inclusions is 5.9%. This results in a slightly higher, 7% relative uncertainty on the mass ratio determination since the Al_2O_3 content of the clinopyroxene is 2.28–3.68 wt%. This 7% relative uncertainty on the mass ratio was considered in the calculation of the uncertainties of element concentrations in the single SMI. It is important to note that the same approach could be used even if the Al_2O_3 content displays a change with melt evolution. In this case the intersection of the trend line from the plagioclase and olivine hosted SMI and the modeled line with various x values would define the mass ratio.

6. Data analysis and comparison

Element concentrations in single SMI and their host minerals determined by LA-ICPMS and associated uncertainties are shown in electronic annex EA-1.

6.1. Data analysis

As mentioned above SMI in each mineral show a significant range in composition. This range is likely due to an evolution in the melt composition and this evolution is best monitored by the Rb content of the melt. Rb is highly incompatible in all crystallizing minerals and present in high enough concentration to be characterized with relatively low uncertainties (<12% relative at 1 SD in most melt inclusions). Plots of major and trace element concentrations as a function of Rb are shown on Fig. 8. The data from various hosts overlap over a broad range of Rb concentrations. This confirms our hypothesis that SMI in the various phases were trapped from the same melt over the same interval of its evolution.

To allow direct comparisons between compositions of SMI from the different host minerals, data for each element were fitted by an uncertainty weighted linear regression. The uncertainty of the fit (RSD of parameters "a" and "b" from the fitting equation $y = ax + b$) were also calculated. This regression was used to compare element concentrations (and uncertainties) in SMI from each host mineral at the same degree of melt evolution, i.e., at a Rb content of 10 ppm. It is important to note that middle and heavy REE are below limit of detection in a significant number of the clinopyroxene hosted inclusions. Thus, the uncertainty in

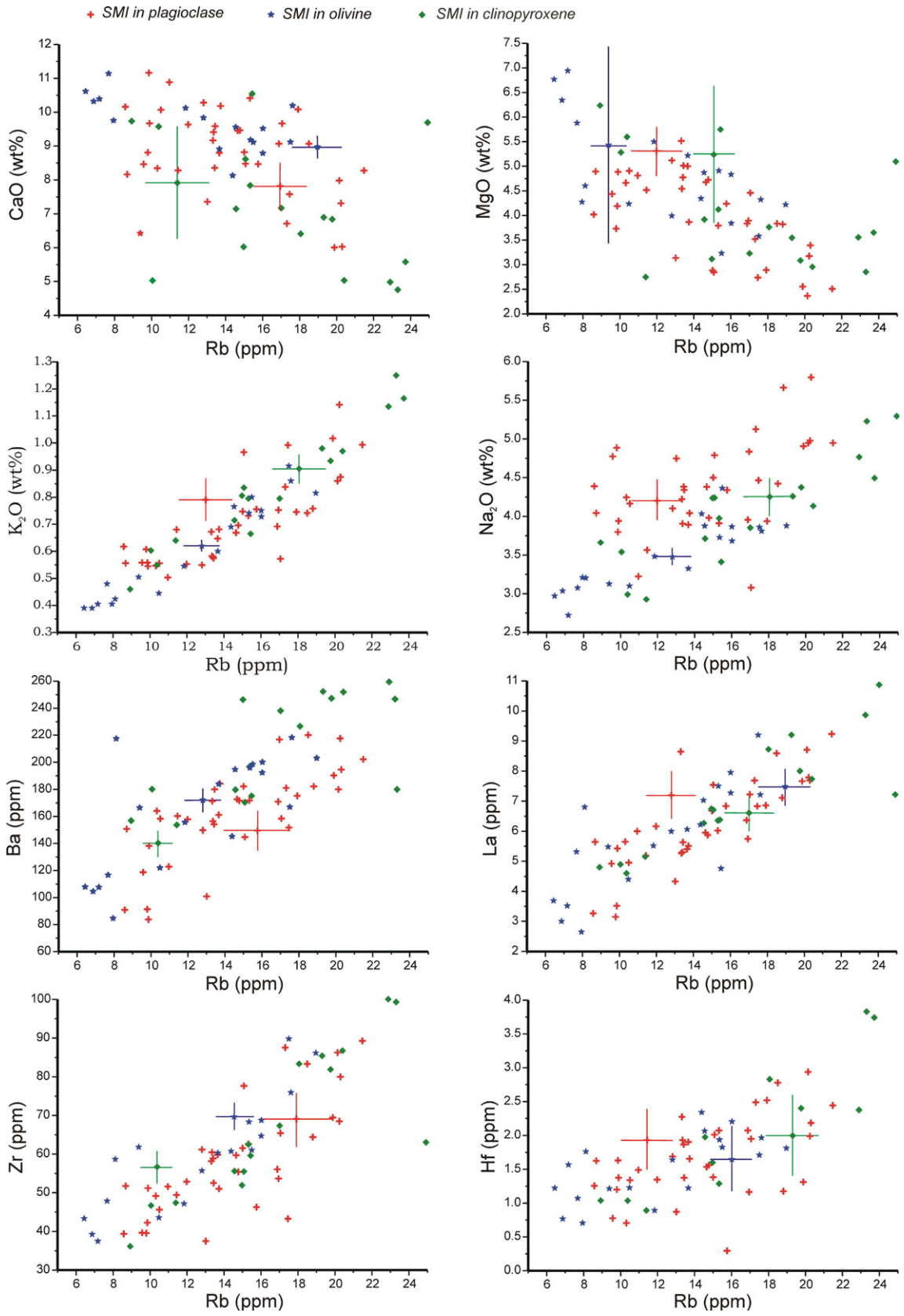

Fig. 8. Selected major and trace element concentrations in SMI analyzed in different host minerals. The error bars show the median uncertainty in the measured concentrations. The tight overlap in the element concentrations indicates that our quantification approach is correct, and that SMI compositions did not suffer significant syn- or postentrapment modification, except for Na_2O in plagioclase hosted SMI.

the fitting for these elements is rather large, strongly exceeding the uncertainty of single SMI analyses. This is further enlarged by the error propagation when calculating the ratio of concentrations in SMI from different host minerals. Li and B concentrations are highly scattering in SMI from each host minerals thus the quality of the fit is also poor for these elements.

The calculated element concentrations in SMI at 10 ppm Rb are shown in Table 3. In Fig. 3 we compared the data on a primitive mantle normalized spider diagram. This comparison shows that the data obtained from SMI of different hosts are in good agreement, and also that the trace element pattern mimics the pattern of the bulk rock. The middle and heavy REE pattern based on the SMI of clinopyroxene is not smooth which is likely due to the higher uncertainty of the data. However, the absolute values scatter around those obtained from the plagioclase and olivine hosted SMI.

In Fig. 9, absolute concentrations of each element in SMI from each host mineral are compared on logarithmic plots. In Fig. 10, ratios of the element concentrations in SMI of different host minerals are shown. It is obvious on both plots that for all elements, except for Cr, Ni, Cu, Na, Y and Sr (see below), concentrations in SMI of the different host minerals are consistent within their 1 SD uncertainty regardless of their absolute concentrations.

Table 3
Major and trace element compositions in SMI trapped in different host minerals

	Plagioclase		Clinopyroxene		Olivine	
	Value at Rb = 10 ppm	Median 1σ uncertainty (%)	Value at Rb = 10 ppm	Median 1σ uncertainty (%)	Value at Rb = 10 ppm	Median 1σ uncertainty (%)
SiO_2	51.8	2	55.6	5	50.9	3
TiO_2	0.65	10	0.55	5	0.68	3
Al_2O_3	17.2	9	16.9	5	17.3	3
FeO	6.9	9	6.9	5	7.8	8
MnO	0.13	10	0.12	7	0.11	9
MgO	4.6	10	5.3	27	5.3	38
CaO	9.9	9	8.9	21	9.9	3
Na_2O	3.9	6	3.2	6	3.2	3
K_2O	0.55	10	0.54	6	0.51	3
P	373	10	457	7	498	5
Sc	32	11	31	34	30	7
V	205	10	219	8	212	4
Cr	86	18	512	23	159	18
Ni	20	33	51	37	425	23
Cu	521	10	55	9	86	8
Rb	10.0	11	10.0	8	10.0	8
Sr	381	8	452	6	406	3
Y	13.1	11	10.4	10	15.0	6
Zr	45	10	42	7	50	5
Nb	0.78	16	1.03	13	0.85	18
Ba	140	10	150	7	137	5
Cs	0.80	17	0.86	14	0.97	17
La	4.9	12	4.7	9	5.1	9
Ce	12.1	11	13.3	7	12.2	6
Nd	7.0	15	7.6	17	7.8	13
Sm	1.63	24	1.98	32	2.39	27
Eu	0.68	24	0.69	34	0.72	30
Gd	2.21	24	1.63	31	2.14	26
Tb	0.36	25	0.37	30	0.43	24
Yb	1.16	23	1.32	29	1.52	24
Lu	0.22	23	0.20	32	0.24	22
Hf	1.29	24	1.10	30	1.46	27
Ta	0.04	39	0.05	36	0.05	36
Pb	4.6	14	4.8	10	5.5	11
Th	0.73	18	0.90	16	0.72	21
U	0.21	31	0.29	26	0.21	34
Pr	1.41	14	1.57	14	1.49	14
Ho	0.53	21	0.51	26	0.56	22
B	8.4	29	11.6	26	13.2	22
Li	9.0	17	6.6	17	11.5	22

The shown concentrations are the values that the linear trendlines took at Rb = 10 ppm. The uncertainties shown are the median of the uncertainty of each single SMI analyses in the specified host mineral. Major elements in wt%, trace elements in ppm.

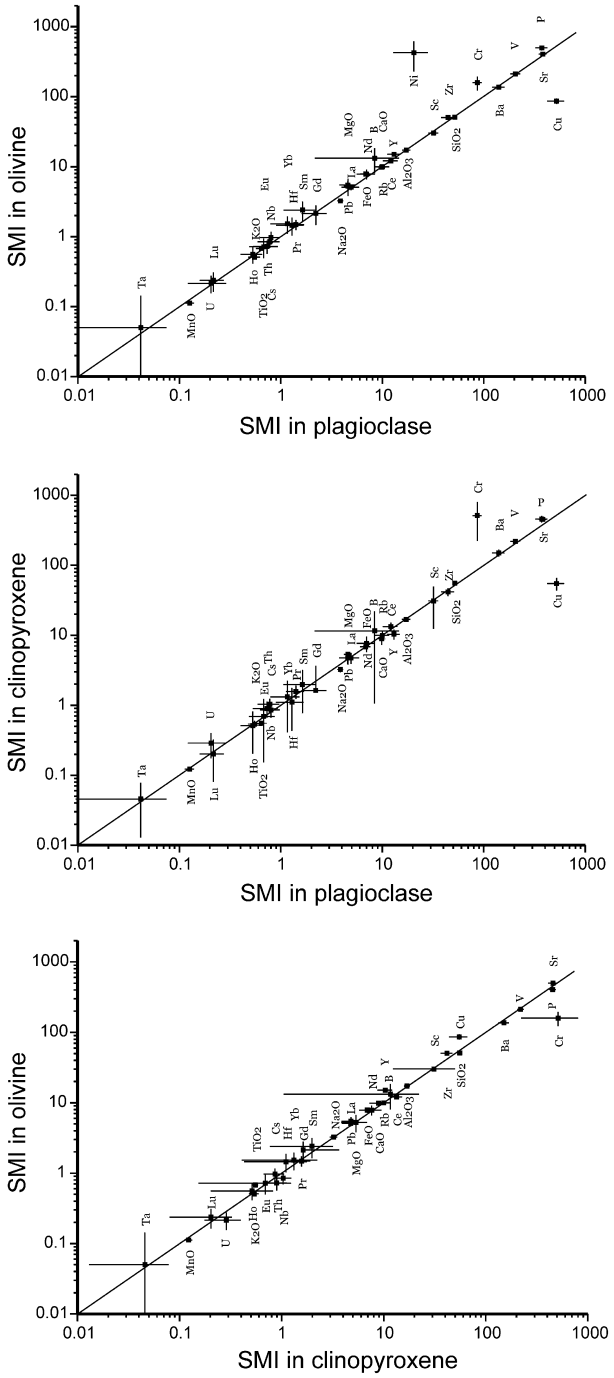

Fig. 9. Comparison of the composition of SMI from different host minerals. The plotted concentrations are the calculated concentrations in the melt at Rb = 10 ppm. Concentration of major elements are plotted in wt% oxides, trace elements are plotted in ppm of the element. Except for Cu, Ni, Cr, Na_2O, Sr and Y all elements have the same abundance regardless of the host mineral. Error bars show the uncertainty of the values at 10 ppm Rb defined by the linear regression. Ni content of clinopyroxene hosted SMI were below limit of detection except for two analyses, thus values at Rb = 10 ppm could have not been calculated.

6.2. Validity of the data

Figs. 9 and 10 show that there is an excellent agreement in the concentrations of most major and trace elements in SMI from various host minerals. This has several implications:

1. To quantify SMI analyses in plagioclase and clinopyroxene, we assumed (based on textural evidence for their cotectic crystallization) that melts entrapped in both minerals show overlapping evolution trends with respect to their Al_2O_3/V ratio and Al_2O_3 content. The good agreement in the concentration of almost all other elements suggests that the assumption is valid. If this assumption had not been correct, the deconvolution of the mixed signal would have been carried out using erroneous mass ratios and the derived SMI compositions would not have been consistent in the different hosts. The only possibility to have consistent concentrations of elements that are compatible in one phase and incompatible in another is to have a mass ratio that is correct and that the phases were indeed co-precipitating.
2. Analytical artifacts such as non-representative sampling, elemental fractionation during ablation, particle transport or ionization are negligible. Errors resulted by such effects would be enlarged by the extrapolation from the mixed signal to the SMI composition. Since there is no discrepancy in the SMI composition we conclude that our analytical approach is valid. This includes the quantification procedure based on the deconvolution of the mixed SMI + host mineral signal.
3. Syn- or postentrapment modification processes did not significantly modify the composition of SMI, these would have resulted in enrichment or depletion of elements as a function of their compatibility. Since even elements which are highly incompatible in one host but compatible in an other show consistent concentrations we suggest that in the present case, SMI compositions have not been significantly modified by boundary layer effects during entrapment or by diffusion processes after entrapment. Thus SMI are a representative sample of the original melt composition with respect to most analytes.

6.3. Potential sources of errors

Cr concentration in some olivine and clinopyroxene hosted SMI are strongly elevated. In olivine the reason for the high Cr-concentrations is likely to be the heterogeneous entrapment of Cr–spinel along with the melt. Cr–spinels are observable in microscopic and BSE images, as well as on the time resolved LA-ICPMS signals through well defined Cr peaks during the ablation of SMI. Wide scattering of the Cr-concentrations in olivine hosted SMI is also primary evidence of heterogeneous entrapment. Data from SMI containing more than 2000 ppm Cr in bulk composition were disregarded since these inclusions contain more than 1 wt% heterogeneously entrapped Cr–spinel and concentration of other elements compatible in Cr–spinel such as V can be significantly modified.

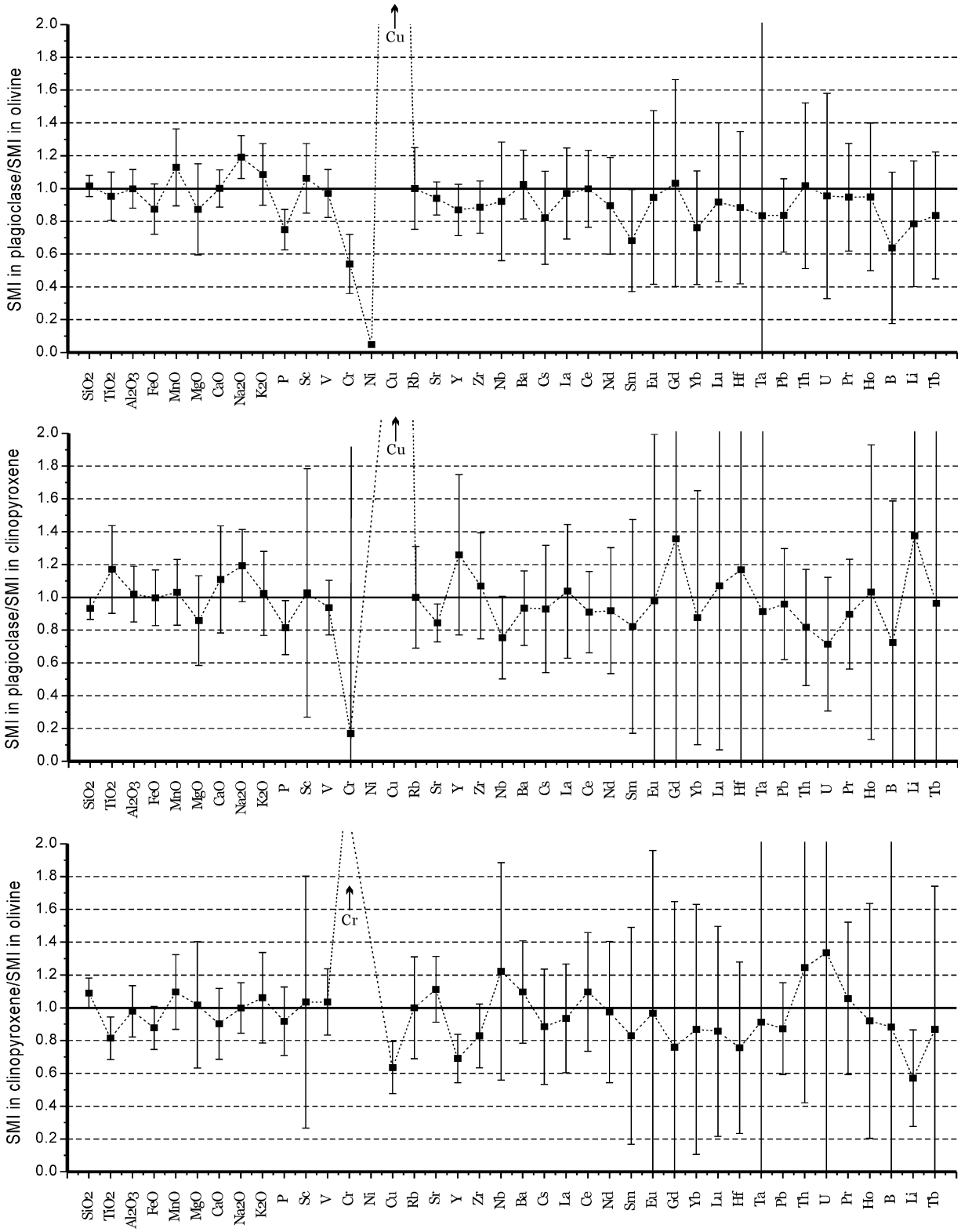

Fig. 10. Ratio of major and trace element concentrations at Rb = 10 ppm between SMI from different host minerals. Error bars are calculated by the propagation of the uncertainty of the values at 10 ppm Rb defined by the linear regression for SMI in each host mineral.

Cr is highly compatible in clinopyroxene and very small heterogeneities in the host mineral can lead to significant errors on the derived SMI composition due to subtraction of inappropriate host mineral composition from the mixed signal. Thus data on Cr concentration in most clinopyroxene hosted inclusions are subject to large uncertainties. For example, an uncertainty of 10% in the Cr-content of the clinopyroxene would typically result in a difference of

700 ppm Cr in the derived SMI composition. In contrast, plagioclase hosted SMI provide very consistent Cr concentration showing good negative correlation with the Rb content or the mg# of the melt (Fig. 11). A negative correlation between two incompatible elements cannot be generated by boundary layer effects. A similar interpretation to Cr in clinopyroxene hosted SMI can be made to account for the variation in the calculated Ni content of olivine hosted SMI.

Cu concentrations in plagioclase hosted inclusions are highly variable and reach extremely high values (up to 5000 ppm). These high Cu concentrations are unlikely to represent true concentrations in melts and are inconsistent with those analyzed in clinopyroxene and olivine hosted SMI. SMI in plagioclase also show variable amounts of excess Na_2O compared to olivine and clinopyroxene hosted SMI (Figs. 8–10). The amount of excess Na_2O for plagioclase hosted SMI was calculated using the Rb versus Na_2O plots, taking the difference between the Na_2O content of each plagioclase hosted SMI and the linear regression from the clinopyroxene hosted SMI. The excess Na_2O correlates with the Cu content in plagioclase hosted SMI (Fig. 12). Thus we suggest that in plagioclase the elevated Cu contents are likely due to heterogeneous entrapment of variable amounts of a fluid phase. Detailed discussion of this process is beyond the scope of this paper and will be published elsewhere. Considering that concentration of the rest of the analytes in the plagioclase hosted SMI are consistent with those hosted by clinopyroxene and olivine, we think that the volume proportion of such a heterogeneously entrapped fluid phase must have been low, and did not contain other analytes in significant concentrations.

Yttrium is present in slightly different concentration in the SMI of different hosts, Sr shows slightly elevated concentration in clinopyroxene hosted SMI. The reasons for these differences are unclear.

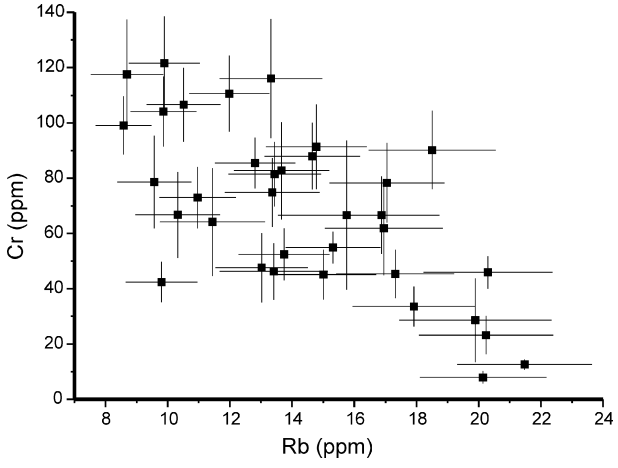

Fig. 11. Rb versus Cr concentration in plagioclase hosted SMI. Error bars are 1σ uncertainties. The negative correlation shows that variations in element concentrations are not induced by boundary layer effect, since Rb and Cr are both incompatible in plagioclase.

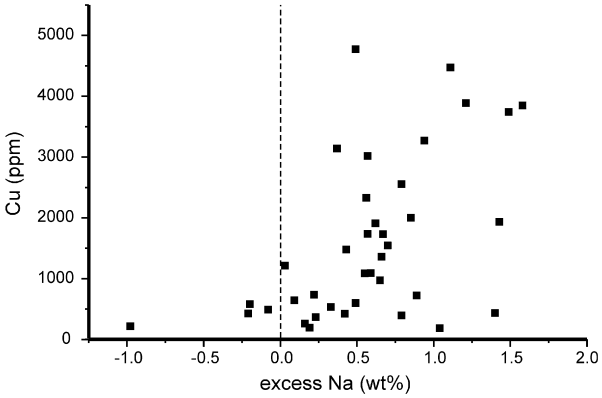

Fig. 12. Correlation of the excess Na_2O in plagioclase hosted SMI with the Cu content. The correlation suggests that selective enrichment of these two elements is due to heterogeneous entrapment of a Cu and Na rich phase, such as a saline fluid.

The above examples of heterogeneous entrapment highlight the critical importance of analyzing a significant number of SMI. As SMI are heterogeneous prior to analysis, accidentally trapped phases cannot be identified petrographically. Thus, the only way that anomalous concentrations due to heterogeneous entrapment can be identified is through analyses of multiple inclusions. Our examples show that this approach is efficient in identifying trapped phases. This also implies that concentration of elements that do not scatter can be considered reliable.

7. Limitations

7.1. Application area

Application of LA-ICPMS is most advantageous in studies focusing on (1) magma chamber processes (rapid analysis of numerous melt inclusions in various host minerals allowing recognition of mixing, assimilation and contamination); (2) melt inclusions trapped at high pressures, for example in early phenocrysts, igneous cumulates and mantle xenoliths (avoiding problems with decrepitation of the SMI or stretching of the host mineral during heating); (3) hydrous melt inclusions, as homogenization experiments are rather difficult in such samples; (4) variations in concentrations of metals of economic importance (often residing in the bubble which can frequently not be redissolved in the melt during heating).

A major limitation of LA-ICPMS analysis of SMI compared to SIMS, and EPMA is that it does not allow analysis of volatile elements (H_2O, Cl, S, CO_2) and isotopic ratios of light elements. In studies focusing on the pre-eruptive volatile content of melts, SIMS and/or EPMA should be the technique of choice. Indeed, homogenization of selected SMI should always be attempted to complement LA-ICPMS data. Vice versa, data obtained on volatile contents or isotopic compositions of homogenized SMI are more meaningful if the conditions at which the SMI were trapped (timing during melt evolution or magma mixing

events) can be well defined. This can easily be done comparing the major and trace element composition of the homogenized SMI to a large dataset produced by LA-ICPMS on unheated SMI. Furthermore, simultaneous application of LA-ICPMS and SIMS/EPMA allows assessment of potential compositional changes during heating experiments. As H_2O contents can be determined by Raman spectroscopy (Zajacz et al., 2005; Behrens et al., 2006; Di Muro et al., 2006; Thomas et al., 2006) all major and trace elements (except for CO_2) can be analyzed with commonly available LA-ICPMS, electron microprobe, and Raman spectroscopy.

Application of the quantification strategies presented here for LA-ICPMS analyses of SMI requires either presence of SMI in at least two co-precipitating mineral or the presence of SMI in olivine. These conditions are met in most igneous rocks, since most magmas have cotectic phase assemblages along a major part of the liquid line of descent apart from near liquidus conditions (Foden and Green, 1992; Moore and Carmichael, 1998; Grove et al., 2003; Holtz et al., 2005). In a large portion of basaltic and basaltic andesitic rocks, at crustal pressures, olivine is the first mineral to appear on the liquidus (Foden and Green, 1992; Moore and Carmichael, 1998; Danyushevsky, 2001; Grove et al., 2003), thus SMI trapped all along the liquid line of descent can be analyzed. Quantification of SMI analyses in orthopyroxene could be done similarly to olivine hosted inclusions with the use of Fe^{2+}/Mg exchange coefficients however it has not been tested in this study.

In rocks formed by magma mixing, identification of co-precipitating mineral pairs has to be done very carefully since phenocrysts from different magmas can co-exist in the same rock. In this case, intergrowth of two mineral phases provides the only clear evidence of their co-precipitation. If intergrowths are rare, or intergrown crystals do not contain an adequate number of SMI, the composition of the intergrown phenocrysts can be analyzed and their composition can be used to identify which SMI-rich, individual phenocrysts were co-precipitated. Subsequently analyses of SMI in these phenocryst populations can be quantified and the composition of the end member melts determined. As an alternative to the intergrowth of minerals, mineral/mineral or mineral/melt equilibrium known from experimental studies can also be used to identify co-precipitating minerals (Streck et al., 2005).

8. Comparison with bulk rock compositions

SMI represent the residual melt in the magma at the time of their entrapment. Bulk rocks are composed of the residual melt and different phenocrysts the amount of which can be selectively decreased by fractionation or increased by accumulation. In a hypothetical closed system, in case of efficient fractionation, trends in bulk rock compositions will overlap with the composition of SMI, while at perfect equilibrium crystallization most SMI will show more evolved compositions than the bulk rocks. In opened systems, however, bulk rock compositions are further modified compared to the magma by assimilation and contamination processes or degassing. In case of magma mixing, SMI will represent the evolution of the melt phase of each magma existing before and after the mixing event. Since this is a methodological study, our aim was to select a system with a simple evolution, characterized by nearly fractional crystallization showing no evidence of magma mixing, so that comparison to bulk rock data can be used to check the quality of the SMI analyses.

In Fig. 13 we compared the composition of SMI with the composition of Villarrica lavas from Hickey-Vargas et al. (2004). Agreement between the composition of bulk rocks and the composition of SMI is very good for Al_2O_3, MgO, CaO and K_2O. However SMI have lower abundances of Fe_2O_3, P_2O_5 and TiO_2. The Na_2O content of the olivine and clinopyroxene hosted SMI closely resemble that of the whole rocks but are elevated in plagioclase hosted SMI for the reasons mentioned above.

Danyushevsky et al. (2002) reported that FeO and TiO_2 depletion in MORB plagioclase hosted inclusions is likely due to modification by syn- or postentrapment diffusion of these elements. Michael et al. (2002) also reported significant TiO_2 and HFSE depletion in MORB plagioclase hosted SMI and attributed this mainly to synentrapment modification of the melt composition due to entrapment in a continuous cycle of growth and dissolution of the host plagioclase. Similar scenarios in the present case are, however, unlikely considering that SMI have consistent Fe_2O_3, TiO_2 and P_2O_5 concentrations regardless to their host mineral. The FeO/MgO ratios in SMI in plagioclase (which is a nearly inert host for these elements) are in equilibrium with the olivine compositions at the estimated redox conditions. This is further evidence that the determined FeO concentrations are representative of the melt.

It is important to note that most lavas investigated from Villarrica in previous studies contain a population of phenocrysts of more evolved composition: olivines with mg# between 72 and 80 and plagioclases with a bimodal distribution of the An content, clustering in the range of 58–66 and 78–84 (Hickey-Vargas et al., 2004). The bimodal distributions of the plagioclase composition has been attributed to a sudden drop in the An content due to ascent and degassing of the magma. The rock investigated in this study mainly contains phenocrysts crystallized at depth at high pH_2O with only a very narrow rim of low Ca/Na (An_{60-70}) overgrowth on the plagioclase crystals. This implies that transportation and quenching of the parental magma happened relatively quickly after leaving the deeper crustal reservoir. Furthermore, the high mg# of the olivine (87–78) and the clinopyroxene (85–79), high Cr-contents of the clinopyroxene (0.8–0.2 wt%) and abundant occurrences of Cr-rich spinel inclusions in olivine also suggest that cores of the investigated phenocrysts crystallized near the liquidus of a primitive magma under the Villarrica volcano.

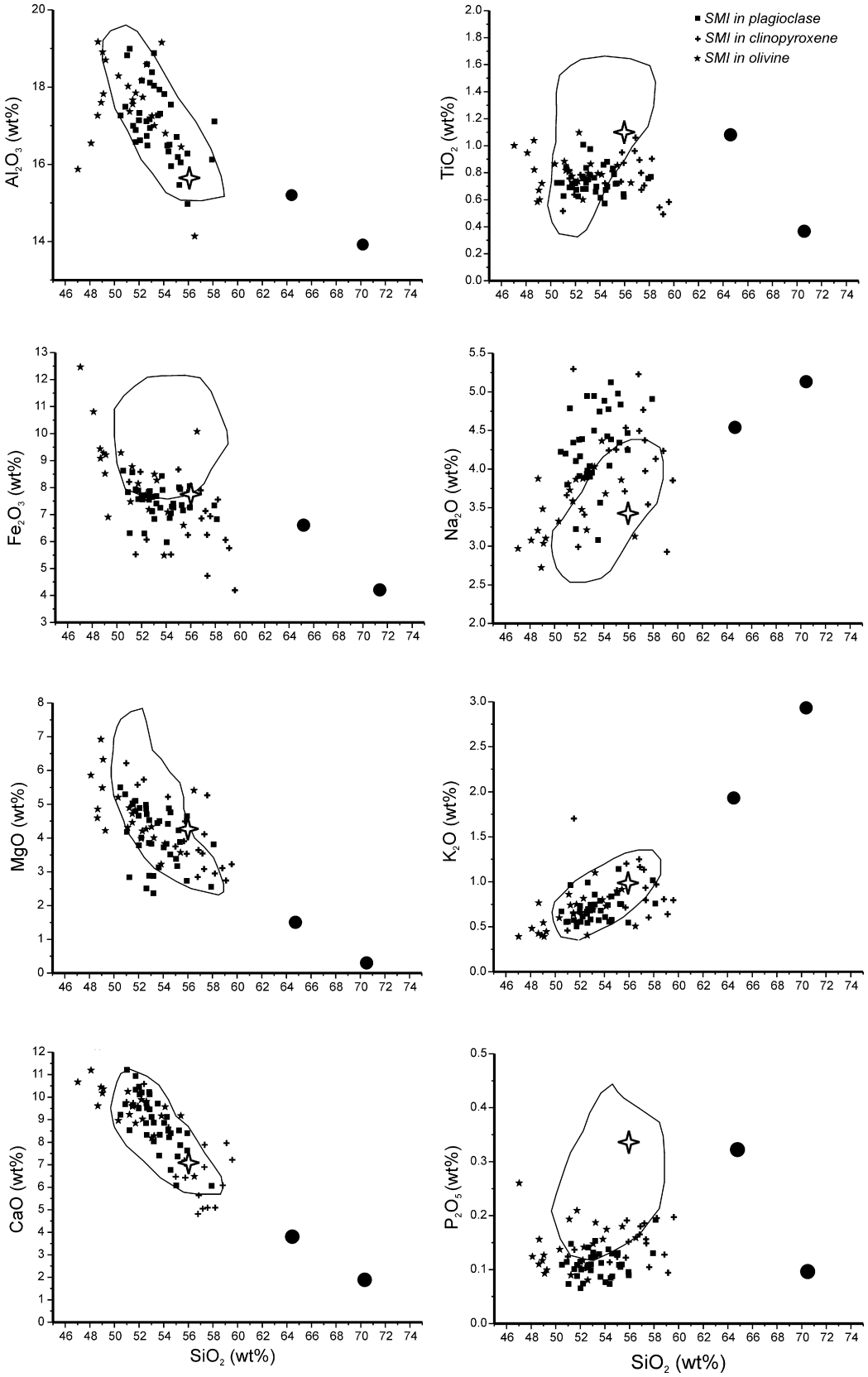

Fig. 13. Comparison of element concentrations in SMI with the compositional field covered by bulk rocks from lava flows of the Villarrica Volcano. The large open stars show the bulk composition of the studied rock sample. The large dots indicate compositions of two cogenetic rocks from Villarica which display significantly more evolved composition than most of the volcanic rocks.

Accordingly, the studied rock represents a quenched primitive magma which evolved mostly at moderate crustal pressure prior to eruption. This contrasts with most Villarrica-lavas which underwent a significant interval of crystallization, and degassing at low pressure. This likely results in slight differences in fractional crystallization processes, which could explain differences in the FeO, P_2O_5 and TiO_2 content compared to most surface volcanic rocks.

As shown in Fig. 3, trace element patterns of SMI closely mimic those of the bulk lavas, even though the absolute concentrations of incompatible trace elements are generally higher in the bulk rocks, than in the more primitive melt inclusions. Sc, V and Sr show only a slight difference due to their compatible behaviour in some of the crystallizing minerals.

In Fig. 14 we compare the Rb content of the SMI with the host phenocrysts compositions to see if their chemical variability correlates with the melt evolution. Correlations can be observed with the An content of the plagioclase and the mg# of the clinopyroxene while the trend in olivine is likely blurred by Fe–Mg diffusion in the crystal lattice. The concentration of most incompatible trace elements, such as Rb, is increasing by a factor of 3 while host phenocrysts compositions display a relatively narrow range. The observed enrichment in incompatible trace element concentrations would require 66% of crystallization in the case of a closed system evolution. This is very unlikely considering the narrow range of phenocryst compositions. Stable and long lived radiogenic isotope studies on Villarrica lavas concluded that crustal contamination processes in the history of this lavas are subordinate (Hickey-Vargas et al., 1989, 2004). However, more recent studies on short lived radiogenic isotopes suggested that contamination or assimilation of cogenetic felsic rocks, crystallized earlier in the crust, is likely (Sun, 2001; Hickey-Vargas et al., 2004). Partial remelting and assimilation of such rocks could explain the rapid increase in trace element concentrations with relatively small change in the major element content of the melt and phenocrysts composition.

We conclude that SMI compositions compare well with the bulk lava compositions from Villarrica Volcano. They represent a primitive batch of magma, crystallizing in the crust at high p_{H_2O}, and likely monitor the interaction with earlier, solidified cogenetic but more felsic magmas.

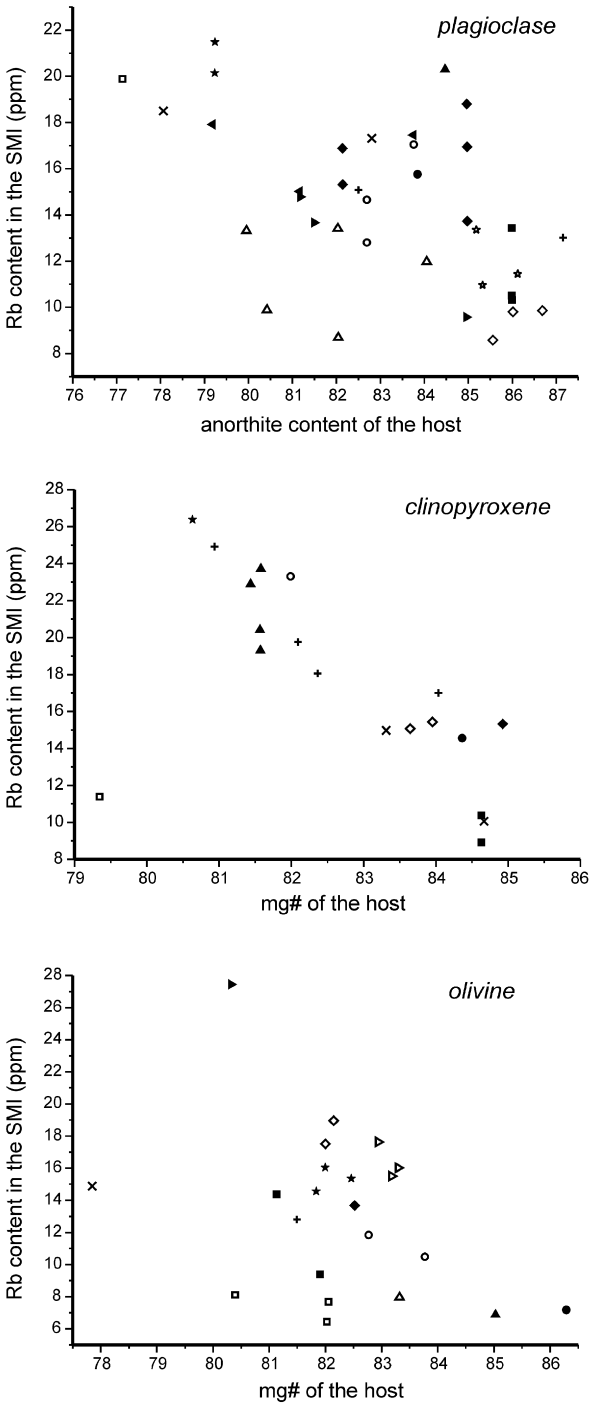

Fig. 14. Rb contents of the SMI as a function of the composition of the host phenocrysts. Same symbols represent SMI measurements from the same crystals. Correlation between the composition of the host mineral and SMI in plagioclase and clinopyroxene is obvious and indicates that the evolution in the melt composition, revealed by the SMI, corresponds to the variation in the composition of the host minerals.

9. Partition coefficients

Simultaneous analysis of SMI and their host mineral provides an opportunity to determine mineral/melt partition coefficients for each analyte. The use of SMI has the advantage of granting equilibrium between the melt and the mineral, a condition that cannot always be verified for partition coefficients based on analysis of magmatic phenocrysts and their matrix glass.

We determined the partition coefficients for each SMI analysis in plagioclase and clinopyroxene, along with their uncertainties using error propagation. In the host olivine, most trace elements were below the limits of detection thus partition coefficients could not be calculated. Concentration of highly incompatible elements were often below limit of detection in the other host minerals too, thus the number of partition coefficients that could be calculated is lower

than the number of inclusions analyzed. Data calculated from less than five data points were disregarded.

We checked for each element if partition coefficients depict a systematic variation along the liquid line of descent by plotting them against the Rb content of the specific SMI. Since no trends are apparent, uncertainty weighted averages of the partition coefficients could be calculated for each element. The uncertainties of the average values are given by the RSD of the single partition coefficients. Average partition coefficients are shown in Table 4.

To check the validity of the set of partition coefficients we fitted them with the model of (Blundy and Wood, 1994; Wood and Blundy, 1997) describing the dependence of partition coefficients on cation charges, effective ionic radii and elasticity of the crystal lattice sites. Effective ionic radii for each cation were taken from (Shannon, 1976). Fig. 15 shows that the model fits our data well with the exception of Ba and Pb in clinopyroxene. Deviant behaviour of Pb and Ba was also found by (Wood and Blundy, 1997) and in the case of Pb^{2+} it was attributed to its non-spherical nature.

The consistency of the partition coefficients with the theoretical model further supports the quality of our data and shows that LA-ICPMS analysis of SMI is an appropriate tool to determine partition coefficients in natural systems.

Table 4
Mineral/melt partition coefficients

	Plagioclase/melt		Clinopyroxene/melt	
	Partition coefficient	1σ uncertainty	Partition coefficient	1σ uncertainty
Ti	0.029	0.008	0.481	0.087
Al	1.84	0.14	0.172	0.020
Mn	0.042	0.008	1.25	0.22
Mg	0.032	0.008	3.75	1.03
Ca	1.72	0.29	2.77	0.75
Na	0.42	0.09	0.075	0.009
K	0.050	0.011	0.0021	0.0012
P	0.094	0.032	0.053	0.016
Sc	0.015	0.007	4.11	0.72
V	0.016	0.005	1.14	0.24
Cu			0.038	0.013
Rb	0.0095	0.0055	0.0045	0.0017
Sr	1.71	0.18	0.065	0.005
Y	0.0110	0.0036	0.698	0.147
Zr	0.0051	0.0024	0.105	0.024
Nb			0.021	0.005
Ba	0.143	0.026	0.0005	0.00004
La	0.072	0.020	0.067	0.023
Ce	0.055	0.014	0.114	0.035
Pr	0.055	0.020	0.197	0.069
Nd	0.043	0.013	0.285	0.075
Sm	0.039	0.017	0.502	0.210
Eu	0.258	0.120	0.600	0.198
Gd	0.038	0.018	0.685	0.231
Tb			0.570	0.122
Ho			0.681	0.169
Yb			0.625	0.102
Lu			0.486	0.148
Hf			0.213	0.111
Pb	0.117	0.036	0.043	0.018
Th			0.0089	0.0013
Li			0.094	0.043

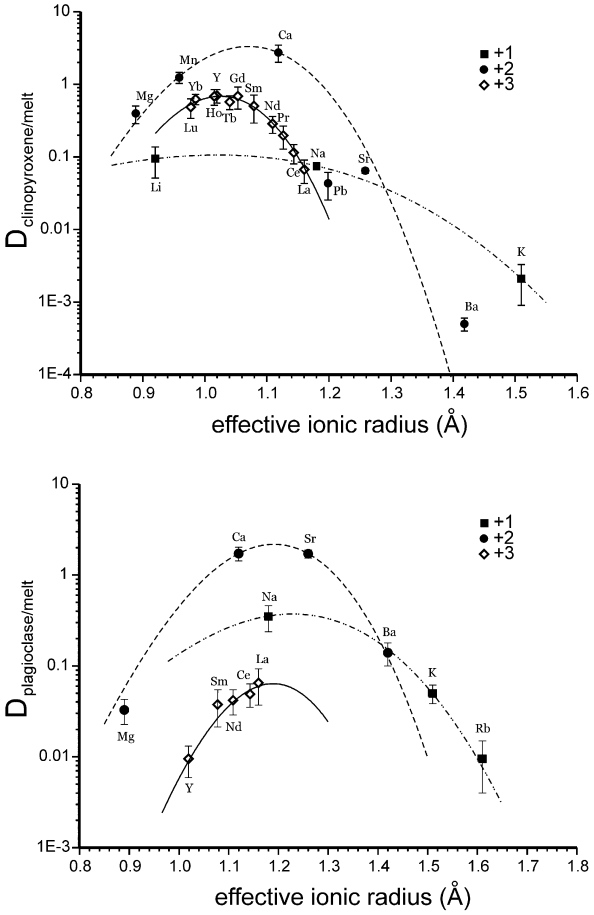

Fig. 15. Mineral/melt partitioning data calculated using the SMI and host mineral compositions as a function of effective ionic radius. Lines represent the fit obtained by the theoretical model of Blundy and Wood (1994).

10. Conclusions

We optimized the use of LA-ICPMS to analyze unheated SMI by developing independent approaches avoiding the use of any additional information or hypothesis on the melt composition. One approach builds on the analysis of SMI in co-precipitated magmatic phenocrysts and quantifies their compositions by assuming overlapping trends in the concentration of selected elements. In the second approach, we use the Fe–Mg exchange between olivine and melt for quantification of SMI in olivine. These approaches provide a unique tool to determine the composition of SMI that cannot be homogenized and the partition coefficients between these melts and minerals. The methods presented here are widely applicable, and can be used over an extended interval of the liquid line of descent in most magmatic rocks.

Similar melt compositions derived from various host phases imply that SMI are indeed representative of the melt

from which the host mineral formed. Any postentrapment modification or boundary layer effect would affect melt compositions in different way in different host minerals. Thus, melt inclusions provide direct and representative information on melts present in a magmatic systems and processes involved in their evolution. Our new approach enables the investigation of melt inclusions in a much larger variety of systems than previously accessible.

Acknowledgments

The authors thank Thomas Pettke and Marcel Guillong for introduction to the principles and usage of LA-ICPMS and the useful discussions about the analytical approach later on. We thank Frederick J. Ryerson and Andreas Audétat for the helpful detailed reviews of the manuscript, and an anonymous reviewer for providing strong motivation to outline better the applicability of our approach. We also thank Martin Streck and Wim Malfait for helpful discussions during our work. This research was supported by the Swiss National Science Foundation (SNF). The project number is PP002-68687.

Associate editor: F.J. Ryerson

Appendix A. Supplementary data

Supplementary data associated with this article can be found, in the online version, at doi:10.1016/j.gca.2006.11.001.

References

Audetat, A., 2000. Quantitative analysis of melt and fluid inclusions by LA-ICP-MS: Practical aspects and selected results. *Acta Petrol. Sin.* **16**, 715.

Audetat, A., Günther, D., Heinrich, C.A., 2000. Magmatic-hydrothermal evolution in a fractionating granite: A microchemical study of the Sn-W-F-mineralized Mole Granite (Australia). *Geochim. Cosmochim. Acta* **64**, 3373–3393.

Ballhaus, C., Berry, R.F., Green, D.H., 1991. High-Pressure Experimental Calibration of the Olivine-Ortho-Pyroxene-Spinel Oxygen Geobarometer - Implications for the Oxidation-State of the Upper Mantle. *Contrib. Mineral. Petr.* **107**, 27–40.

Behrens, H., Roux, J., Neuville, D.R., Siemann, M., 2006. Quantification of dissolved H_2O in silicate glasses using confocal microRaman spectroscopy. *Chem. Geol.* **229**, 96–112.

Blundy, J., Wood, B., 1994. Prediction of crystal-melt partition-coefficients from elastic-moduli. *Nature* **372**, 452–454.

Danyushevsky, L.V., 2001. The effect of small amounts of H_2O crystallisation of mid-ocean ridge and backarc basin magmas. *J. Volcanol. Geoth. Res.* **110**, 265–280.

Danyushevsky, L.V., Della-Pasqua, F.N., Sokolov, S., 2000. Re-equilibration of melt inclusions trapped by magnesian olivine phenocrysts from subduction-related magmas: petrological implications. *Contrib. Mineral. Petrol.* **138**, 68–83.

Danyushevsky, L.V., McNeill, A.W., Sobolev, A.V., 2002. Experimental and petrological studies of melt inclusions in phenocrysts from mantle-derived magmas: an overview of techniques, advantages and complications. *Chem. Geol.* **183**, 5–24.

Di Muro, A., Villemant, B., Montagnac, G., Scaillet, B., Reynard, B., 2006. Quantification of water content and speciation in natural silicic glasses (phonolite, dacite, rhyolite) by confocal microRaman spectrometry. *Geochim. Cosmochim. Acta* **70**, 2868–2884.

Foden, J.D., Green, D.H., 1992. Possible role of amphibole in the origin of andesite—Some experimental and natural evidence. *Contrib. Mineral. Petrol.* **109**, 479–493.

Grove, T.L., Elkins-Tanton, L.T., Parman, S.W., Chatterjee, N., Muntener, O., Gaetani, G.A., 2003. Fractional crystallization and mantle-melting controls on calc-alkaline differentiation trends. *Contrib. Mineral. Petrol.* **145**, 515–533.

Guillong, M., Gunther, D., 2002. Effect of particle size distribution on ICP-induced elemental fractionation in laser ablation-inductively coupled plasma-mass spectrometry. *J. Anal. Atom. Spectrom.* **17**, 831–837.

Guillong, M., Horn, I., Gunther, D., 2003a. A comparison of 266 nm, 213 nm and 193 nm produced from a single solid state Nd: YAG laser for laser ablation ICP-MS. *J. Anal. Atom. Spectrom.* **18**, 1224–1230.

Guillong, M., Kuhn, H.R., Gunther, D., 2003b. Application of a particle separation device to reduce inductively coupled plasma-enhanced elemental fractionation in laser ablation-inductively coupled plasma-mass spectrometry. *Spectrochim. Acta B* **58**, 211–220.

Günther, D., Frischknecht, R., Heinrich, C.A., Kahlert, H.J., 1997. Capabilities of an Argon Fluoride 193 nm excimer laser for laser ablation inductively coupled plasma mass spectrometry microanalysis of geological materials. *J. Anal. Atom. Spectrom.* **12**, 939–944.

Günther, D., Audetat, A., Frischknecht, R., Heinrich, C.A., 1998. Quantitative analysis of major, minor and trace elements in fluid inclusions using laser ablation inductively coupled plasma mass spectrometry. *J. Anal. Atom. Spectrom.* **13**, 263–270.

Günther, D., Heinrich, C.A., 1999a. Comparison of the ablation behaviour of 266 nm Nd: YAG and 193 nm ArF excimer lasers for LA-ICP-MS analysis. *J. Anal. Atom. Spectrom.* **14**, 1369–1374.

Günther, D., Heinrich, C.A., 1999b. Enhanced sensitivity in laser ablation-ICP mass spectrometry using helium–argon mixtures as aerosol carrier— Plenary lecture. *J. Anal. Atom. Spectrom.* **14**, 1363–1368.

Günther, D., Bleiner, D., Guillong, M., Hattendorf, B., Horn, I., 2001. Access to isotopic and elemental composition and their distribution in solid materials by laser ablation-inductively coupled plasma-mass spectrometry. *Chimia* **55**, 778–782.

Halter, W.E., Pettke, T., Heinrich, C.A., Rothen-Rutishauser, B., 2002. Major to trace element analysis of melt inclusions by laser-ablation ICP-MS: methods of quantification. *Chem. Geol.* **183**, 63–86.

Hickey-Vargas, R., Roa, H.M., Escobar, L.L., Frey, F.A., 1989. Geochemical Variations in Andean Basaltic and Silicic Lavas from the Villarrica-Lanin Volcanic Chain (39.5-Degree-S)—an Evaluation of Source Heterogeneity, Fractional Crystallization and Crustal Assimilation. *Contrib. Mineral. Petrol.* **103**, 361–386.

Hickey-Vargas, R., Escobar, L.L., Moreno, H., Clavero, J., Lara, L., Sun., M., 2004. Magmatic evolution of the Villarrica Volcano. In: Lara LaC, J. (Ed.), Subdireccion Nacional De Geolgia, vol. 61. Santiago, p. 73.

Holtz, F., Sato, H., Lewis, J., Behrens, H., Nakada, S., 2005. Experimental petrology of the 1991–1995 Unzen dacite, Japan. Part I: Phase relations, phase composition and pre-eruptive conditions. *J. Petrol.* **46**, 319–337.

Jochum, K.P., Willbold, M., Raczek, I., Stoll, B., Herwig, K., 2005. Chemical characterisation of the USGS reference glasses GSA-1G, GSC-1G, GSD-1G, GSE-1G, BCR-2G, BHVO-2G and BIR-1G using EPMA, ID-TIMS, ID-ICPMS and LA-ICPMS. *Geostandard. Geoanal. Res.* **29**, 285–302.

Kamenetsky, V.S., Eggins, S.M., Crawford, A.J., Green, D.H., Gasparon, M., Falloon, T.J., 1998. Calcic melt inclusions in primitive olivine at 43 degrees N MAR: evidence for melt-rock reaction/melting involving clinopyroxene-rich lithologies during MORB generation. *Earth Planet. Sci. Lett.* **160**, 115–132.

Kress, V.C., Carmichael, I.S.E., 1991. The compressibility of silicate liquids containing Fe_2O_3 and the effect of composition, temperature, oxygen fugacity and pressure on their redox states. *Contrib. Mineral. Petrol.* **108**, 82–92.

Lowenstern, J.B., 1995. Applications of silicate melt inclusions to the study of magmatic volatiles. In: Thompson J.F.H. (Ed.), Magmas, Fluids, and Ore Deposits, vol Short Course, vol. 23, Minerological Association of Canada, Victoria, pp. 71–101.

Michael, P.J., McDonough, W.F., Nielsen, R.L., Cornell, W.C., 2002. Depleted melt inclusions in MORB plagioclase: messages from the mantle or mirages from the magma chamber? *Chem. Geol.* **183**, 43–61.

Moore, G., Carmichael, I.S.E., 1998. The hydrous phase equilibria (to 3 kbar) of an andesite and basaltic andesite from western Mexico: constraints on water content and conditions of phenocryst growth. *Contrib. Mineral. Petrol.* **130**, 304–319.

Pettke, T., Halter, W.E., Webster, J.D., Aigner-Torres, M., Heinrich, C.A., 2004. Accurate quantification of melt inclusion chemistry by LA-ICPMS: a comparison with EMP and SIMS and advantages and possible limitations of these methods. *Lithos* **78**, 333–361.

Rocholl, A., 1998. Major and trace element composition and homogeneity of microbeam reference material: Basalt glass USGS BCR-2G. *Geostandard. NewsLett.* **22**, 33–45.

Schiano, P., 2003. Primitive mantle magmas recorded as silicate melt inclusions in igneous minerals. *Earth-Sci. Rev.* **63**, 121–144.

Shannon, R.D., 1976. Revised effective ionic-radii and systematic studies of interatomic distances in halides and chalcogenides. *Acta Crystallogr. A* **32**, 751–767.

Sisson, T.W., Grove, T.L., 1993a. Experimental investigations of the role of H_2O in calc-alkaline differentiation and subduction zone magmatism. *Contrib. Mineral. Petrol.* **113**, 143–166.

Sisson, T.W., Grove, T.L., 1993b. Temperatures and H_2O contents of low-Mgo high-alumina basalts. *Contrib. Mineral. Petrol.* **113**, 167–184.

Streck, M.J., Dungan, M.A., Bussy, F., Malavassi, E., 2005. Mineral inventory of continuously erupting basaltic andesites at Arenal volcano, Costa Rica: implications for interpreting monotonous, crystal-rich, mafic arc stratigraphies. *J. Volcanol. Geoth. Res.* **140**, 133–155.

Sun, M., 2001. Geochemical variation among small eruptive centers in the Central SVZ of the Andes: An evaluation of subduction, mantle and crustal influences. Ph.D. Thesis, Miami, Florida International University, 292 p.

Taylor, R.P., Jackson, S.E., Longerich, H.P., Webster, J.D., 1997. In situ trace-element analysis of individual silicate melt inclusions by laser ablation microprobe inductively coupled plasma-mass spectrometry (LAM-ICP-MS). *Geochim. Cosmochim. Acta* **61**, 2559–2567.

Thomas, R., Kamenetsky, V.S., Davidson, P., 2006. Laser Raman spectroscopic measurements of water in unexposed glass inclusions. *Am. Mineral.* **91**, 467–470.

Ulmer, P., 1989. The dependence of the Fe^{2+}-Mg Cation-Partitioning between Olivine and Basaltic Liquid on Pressure, Temperature and Composition - an Experimental-Study to 30 Kbars. *Contrib. Mineral. Petrol.* **101**, 261–273.

Wood, B.J., Blundy, J.D., 1997. A predictive model for rare earth element partitioning between clinopyroxene and anhydrous silicate melt. *Contrib. Mineral. Petrol.* **129**, 166–181.

Zajacz, Z., Halter, W., Malfait, W.J., Bachmann, O., Bodnar, R.J., Hirschmann, M.M., Mandeville, C.W., Morizet, Y., Muntener, O., Ulmer, P., Webster, J.D., 2005. A composition-independent quantitative determination of the water content in silicate glasses and silicate melt inclusions by confocal Raman spectroscopy. *Contrib. Mineral. Petrol.* **150**, 631–642.